Detailed studies of the density of states of amorphous NbSi obtained by synchrotron radiation photoemission

1992 J. Phys.: Condens. Matter 4 1131

(http://iopscience.iop.org/0953-8984/4/4/023)

J. Phys.: Condens. Matter 4 (1992) 1131–1141. Printed in the UK

Detailed studies of the density of states of amorphous NbSi obtained by synchrotron radiation photoemission

P K Hucknall†, C G H Walker†, D Greig†, J A D Matthew‡, D Norman§ and J Turton†

† Department of Physics, University of Leeds, Leeds LS2 9JT, UK
‡ Department of Physics, University of York, York YO1 5DD, UK
§ SERC Daresbury Laboratory, Daresbury, Warrington WA4 4AD, UK

Received 23 July 1991, in final form 8 October 1991

Abstract. Ultraviolet photoemission experiments using radiation from a synchrotron source have been used to study details of the valence bands of amorphous Nb_xSi_{1-x} on either side of the metal–insulator transition. The alloys were prepared *in situ* by RF magnetron sputtering with surface and bulk characterization obtained by Auger electron spectroscopy and EXAFS respectively. The variation of the intensities of several features in the UV spectra with photon energy are due to the presence of resonant photoemission and Cooper minima in photoionization, and these effects can be used to identify the atomic origins of the partial densities of states in different parts of the valence bands. In the metallic phase such measurements show 'pure' Nb 4d states close to the Fermi edge, whereas for the insulating material there is no Fermi edge and little evidence for the Nb resonance.

1. Introduction

Metallic glasses may show spectacular variations in their transport properties with alloy composition with particularly dramatic changes taking place at a metal–insulator transition. Such effects are certainly accompanied by corresponding changes in the densities of filled electronic states and the purpose of this paper is to demonstrate the value of tunable synchrotron radiation in studying these changes in the Nb–Si system. The outer electronic states of atomic Nb and Si are $4d^45s^1$ and $3s^23p^2$ respectively, and the amorphous alloy system, Nb_xSi_{1-x}, undergoes a metal–insulator transition at an atomic concentration of about 89% silicon ($x = 0.11$) [1]. Over most of the concentration range the electrical properties of the alloys, both microcrystalline and amorphous, exhibit 'metallic-like' behaviour including evidence of weak localization or quantum interference effects in highly resistive alloys as expected [2, 3]. However, on the insulating side of the transition the electrical transport properties are quite different. At concentrations close to the critical composition the alloys are in the variable range hopping regime where the resistivity should vary as $\exp[(T_0/T)^{1/4}]$, where, for each separate alloy, T_0 is a constant that can be obtained from the experimental data. In addition, the magnetoresistance in this composition range is expected to be negative and proportional to the applied field. For a-NbSi containing between 89 and 91% silicon both of these predictions have recently been confirmed by Pounder and Howson [3].

0953-8984/92/041131+11$04.50

Previous measurements of ultraviolet photoemission spectroscopy (UPS) on these alloys using a fixed frequency HeII source provided the first direct evidence of dramatic changes in the form of the densities of states (DOS) near the Fermi levels on opposite sides of the transition [4]. In this paper we show the value of measurements made with the UK Synchrotron Radiation Source, Daresbury, in studying these effects in much greater detail. In particular we shall demonstrate the importance of several techniques that are made possible by the availability of tunable radiation. The most useful of these is that we then have the facility to study the photoelectric response of electrons at a given binding energy when the specimen is irradiated by photons covering a wide range of energies, and thus obtain spectra in what is generally termed the Constant Initial State (CIS) mode. Any marked variation of photoemission intensity with photon energy may be the result of either Cooper minima or resonances and these important phenomena are central to the experiments.

1.1. Cooper minima

The photoionization cross section for electron excitations from a state $|i\rangle$ within a metal to a continuum state $|k\rangle$ above the vacuum level depends on the matrix element $\langle k|r|i\rangle$. If the eigenstate $|i\rangle$ contains a node as, for example, in the 4d state of Nb, there will be a change of sign of the matrix element for increasing values of k. For certain values of kinetic energies the level of photoionization is therefore extremely small and it is this effect that is known as a Cooper minimum. It is particularly pronounced when there is only one node present; the condition for this is $n = l + 2$—a condition that is satisfied for 4d electrons. The photoionization cross sections of different atomic states in free atoms have been calculated by Yeh and Lindau [5], and it is their results, including the presence of Cooper minima, that are used as the starting point in interpreting the data.

1.2. Resonance photoemission

Some single electron peaks and satellites associated with valence electrons in a photoemission spectrum can undergo resonant enhancement when the photon energy is tuned to excite a core level. The mechanism for this involves autoionization through the super-Coster–Kronig decay of a photohole following resonant excitation; e.g. after np to nd excitations in transition metals or 4d to 4f transitions in Ba or in the rare earths. The final states of the decay process are identical to those of direct photoemission and the interference between the direct and resonant amplitudes controls the resonant profile.

Since both of these effects are atom-specific they can be used to identify the atomic origins of spectral features including details of the partial densities of states, and we have given examples of the use of these techniques elsewhere [6, 7].

2. Experimental details

All the amorphous alloys were formed as thin films on stainless steel substrates by RF magnetron sputtering. Some of the early specimens were produced at Leeds in commercial Ion Tech equipment and cleaned in the experimental chamber at Daresbury by argon ion bombardment, but we later developed a process at Daresbury for *in situ* sputtering in a preparation chamber attached to the experimental ultra-high vacuum

(UHV) chambers. The specimens could thus be transferred into the measurement positions without breaking vacuum and therefore without oxygen contamination.

At both Leeds and Daresbury the sputtering targets were composed of segments made from high purity elements. The base pressures for *ex situ* and *in situ* sputtering were 10^{-7} and 3×10^{-10} mbar respectively, with zero grade and research grade (5*n*.5) argon as the sputtering gases in the two cases. Bulk composition analysis was performed at Leeds using a Cameca Camebox SX50 electron microprobe (EMP), while analyses of the specimens prepared at Daresbury were obtained by Auger electron spectroscopy. As a further test of the quality of the samples and to ensure that they consisted of a single phase we carried out EXAFS studies of a-NbSi in the composition range 2–20 at.% Nb. These studies were performed on station 9.2 at Daresbury by measuring the fluorescence spectra around the Nb K edge at 18 986 eV.

The photoemission and Auger spectra were measured in UHV conditions with the average vacuum about 2×10^{-10} mbar. All data were collected with a double pass angle integrating cylindrical mirror analyser (CMA) on stations 6.1 and 6.2, the former covering the energy range 40–150 eV [8] and the latter 15 to ~80 eV. The resolution measured directly from the observed tantalum Fermi edge varied from about 0.3 eV at 20 eV to 1.2 eV at 150 eV. The spectra shown in this paper have all been normalized to the incident photon fluxes which were monitored continuously by measuring the drain currents from a tungsten grid, while the work functions and binding energy scales have been set by observing the location of the Fermi edge of a tantalum sample in electrical contact with the alloys.

3. Results

3.1. Auger spectra and surface segregation

The photoelectrons and Auger electrons used in our experiments have a mean free path of a few atomic layers. Hence, the UPS spectra are not fully representative of the bulk material. Furthermore, surface contamination will affect both UPS and Auger spectra and it is for this reason that experiments must be carried out under UHV conditions. The samples that were sputtered at Leeds were found to be heavily contaminated with carbon and oxygen on their surfaces and even after cleaning by argon ion bombardment for 2.5 h Auger electron spectroscopy still showed large C and O peaks (see figure 1(*a*)). By way of complete contrast, as can be seen from figures 1(*b*)(i) and 1(*c*)(i), the *in situ* sputtered samples were very clean immediately after sputtering, with no detectable C or O in their Auger spectra.

At regular intervals during the collection of photoemission spectra, Auger scans were taken to monitor the build-up of surface contaminants. Over a period of hours, the surface showed a steady growth of the C and O peaks and so the surface was cleaned regularly by argon ion bombardment. Unfortunately, in this case the argon cleaning not only changed the C and O peaks, but also the relative intensities of the Si LMM (92 eV) and Nb MNN (167 eV) peaks. These changes can be clearly seen in figure 1, and imply an increase in the relative surface concentration of Nb upon argon bombardment.

An approximate quantitative analysis of the Auger spectra using published CMA sensitivity factors was performed on the spectra [9, 10] and compared with the bulk electron microprobe analysis of the same samples (table 1). They suggest that, as Ar bombardment is applied to the sample, the surface concentration which is initially Si

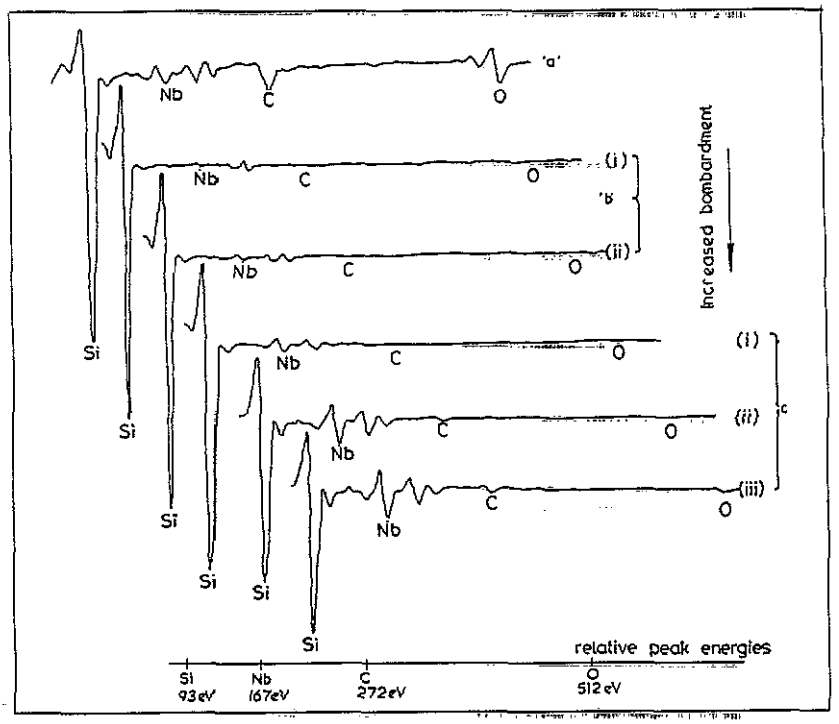

Figure 1. Auger electron spectra with the common energy scale demonstrating the location of the peaks. (*a*) Nb–Si sample sputtered in a separate system and transferred into the UHV chamber after residing in air for 2 days. Spectrum collected after Ar bombardment for 150 min at 4 kV. (*b*) Auger electron spectra of the insulating sample (1.5 at.% Nb). (i) As-sputtered. (ii) After 30 min Ar cleaning at 2 kV. (*c*) Auger electron spectra of the metallic sample (18.0 at.% Nb). (i) As-sputtered. (ii) After 30 min Ar cleaning at 1 kV (soft clean). (iii) After a further 30 min Ar cleaning at 2 kV (hard clean).

rich passes through the bulk concentration and finally becomes rich in Nb. We believe that there are two processes involved. First, during sputter deposition of the NbSi samples a Si rich layer a few monolayers thick forms at the surface due to a tendency of the Nb atoms to embed themselves more deeply into the open sputtered structure than the Si atoms. Second, during Ar^+ bombardment preferential sputtering of the lighter Si atoms may occur, but the fact that specimens of different bulk composition do evolve to different surface compositions on cleaning suggests that preferential sputtering is not completely dominant. This is consistent with estimates of the Si and Nb sputtering rates under comparable conditions. It is quite possible that these variations could also be present in previous measurements of a-NbSi surfaces [4, 11–13].

3.2. EXAFS

The EXAFS data at the Nb edge were collected by 13 GeLi fluorescence detectors and analysed by the EXBACK and EXCURV programs. For details of these programs, developed at Daresbury to determine the coordination, separation and type of atom surrounding the atom whose EXAFS spectrum is being investigated, see [14, 15]. The results show that Nb is entirely coordinated by Si, with no detectable Nb–Nb bonding.

Table 1. Atomic percentage of Nb in the films as determined by Auger and electron microprobe analysis.

	Auger analysis (surface) (%)	Electron microprobe (bulk) (%)
'Metallic'		
as-prepared	5.2	18.5
Lightly cleaned	18.0	—
Heavily cleaned	26.0	—
'Insulating'		
as-prepared	1.4	1.5
Cleaned	2.9	—

An example of an EXAFS spectrum from a sample containing 12 at.% Nb is shown in figure 2 where the single peak is indicative of the amorphous state [15]. The spectra are all described by a one-shell model with Nb–Si distances of 2.65 Å. These results agree with those of Kortright and Bienenstock [16] who studied a similar alloy, a-MoGe, and found that the Mo was predominantly surrounded by six Ge atoms. On the other hand, EXAFS studies of a-SiNiH [17] showed that a two-shell model was required to describe the Ni EXAFS data with one shell of Si and one of Ni at slightly different distances from the central atom. This led to a two-phase model of this particular alloy and is in complete contrast to the present results where no evidence of such a two-phase system has been found.

3.3. Photoemission

Photoemission experiments were performed with the aim of highlighting differences in the partial densities of states of Nb and Si in the metal and insulating phases with particular emphasis on the Fermi level region.

3.4. Metallic against insulating

Two series of energy distribution curves (EDCs) for specimens on either side of the metal–insulator transition are shown in figure 3. For the metallic case shown in figure 3(*a*), there are two features of particular note: (i) the sharp reduction in intensity around zero binding energy, indicating the existence of a Fermi edge—a point that we shall return to later; and (ii) Nb 4p–4d resonant enhancement that can be seen to reach a maximum intensity at about 44 eV, well above the binding energy for Nb 4p electrons (about 29 eV) [18]. The resonating feature is labelled B in figure 3(*a*), and extends from E_F to about 6 eV below E_F. This is in broad agreement with the energy range of the 4d level from previous XPS studies of a-NbSi [4, 11–13] and metal silicides [19–21] although there may be hybridization with Si 3p orbitals. At higher binding energies the resonance is not quite so intense indicating increased p–d hybridization. Feature A in figure 3(*a*) is the Nb $N_{23}VV$ Auger peak.

Figure 3(*b*) shows EDC spectra for the insulating case where, in contrast to figure 3(*a*), there is no Fermi edge and little evidence for the Nb resonance. However, there are two other features which become particularly prominent at low photon energies. At such low Nb concentrations ($\simeq$ 4%) it is anticipated that the density of states will resemble that of amorphous Si [22]. Peak C at 10 eV binding energy is due to the Si 3s-like states and peak D at 7 eV binding energy is due mainly to

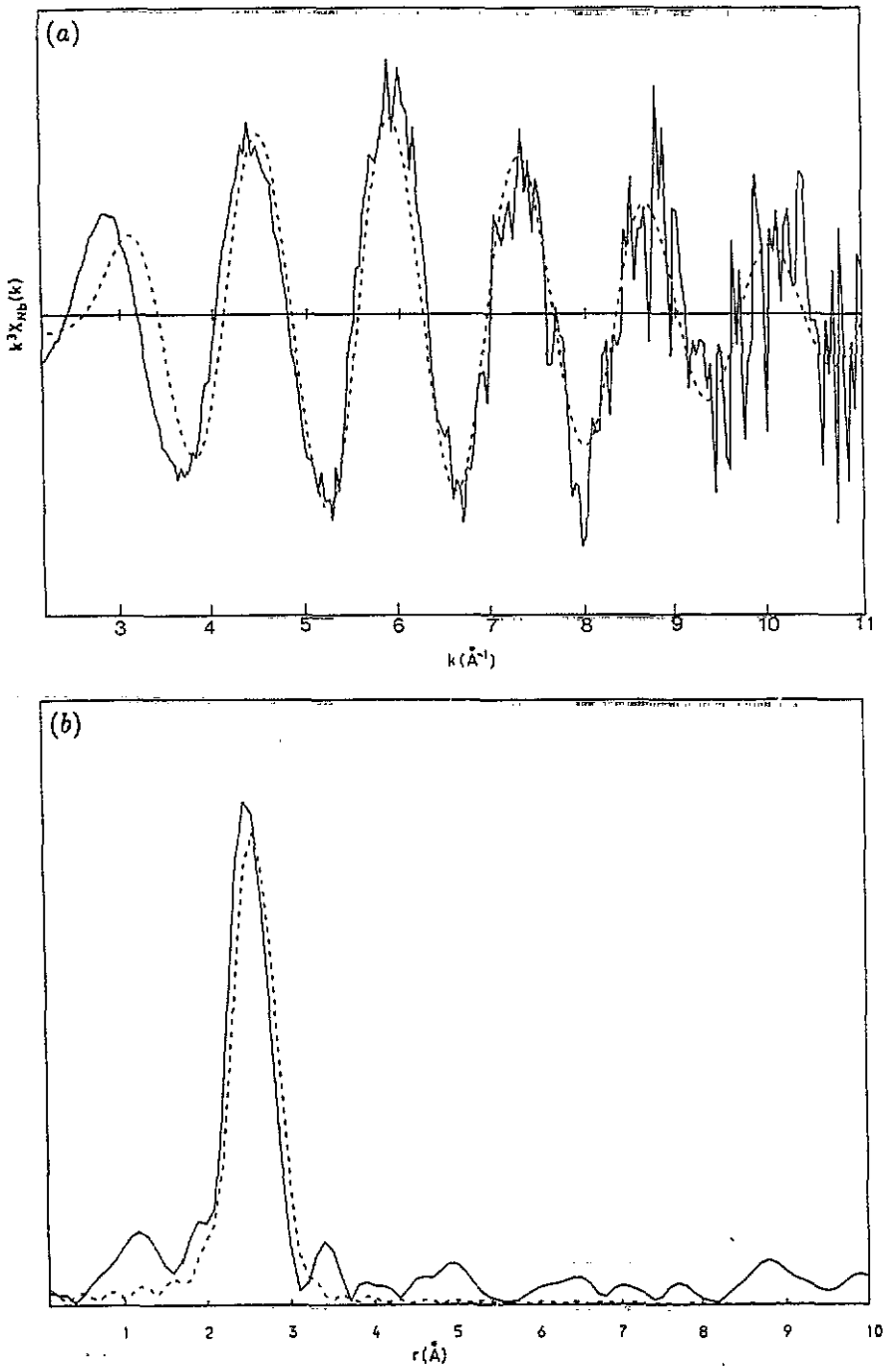

Figure 2. Nb EXAFS from the K shell. (*a*) $k^3\chi(k)$ against k over the range 3–11 Å^{-1} for a $Si_{1-x}Nb_x$ with $x = 0.12$. The full curves are experimental data. The broken curves are theoretical fits using a single shell model. Data for the theoretical fit are: coordination number = 4.783; atom type = Si; distance of shell = 2.65 Å. (*b*) Fourier transform of Nb EXAFS data showing a single shell in both experiment and theory. k = photoelectron wavevector; r = distance from central atom; $\chi(k)$ = EXAFS function, i.e. function that remains after subtraction of pre- and post-edge backgrounds.

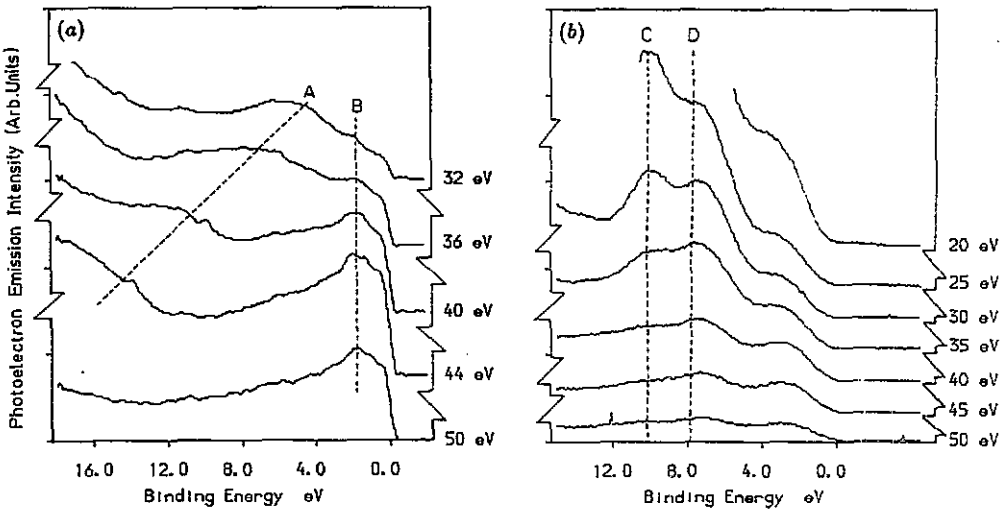

Figure 3. Photoemission: (*a*) EDC scans of the as-sputtered metallic a-NbSi sample (18.0 at.% Nb) acquired using the lower-energy monochromator. Feature B shows the 4p–4d Nb resonance while A is the Nb NVV Auger peak. (*b*) EDC scans of the as-sputtered insulating a-NbSi sample (1.5 at.% Nb). Labels C and D indicate Si 3s and Si 3p states respectively.

the Si 3p states with some 3s admixture. This differs significantly from the partial densities of states predicted for NbSi and Nb_3Si [12] where the peaks in that region have dominantly 3s character. These peaks are not so clearly seen in the spectra from the 'metallic' samples due to the much larger Nb 4d photemission cross section engulfing the Si 3p signal. The binding energies of the Si 3s and 3p peaks are slightly lower than those suggested by Söldner and Saemann-Ischenko [4].

3.5. Partial densities of states

Figure 4 shows the effect of Ar cleaning on the shape of the EDC spectra close to the Fermi edge. Figure 4(*a*) gives the EDC spectrum as a function of Ar exposure for the metallic sample at a photon energy of 60 eV. The sharp rise at the Fermi edge with cleaning is the result of the increased concentration of Nb at the surface. Indeed, according to our crude analysis the sample surface will have passed through the composition corresponding to the M–I transition (see table 1). It is also clear from figure 4(*a*) that the absolute intensity of the valence band feature increases with cleaning. This is due to the higher concentration of Nb and the higher photoemission cross section of the Nb 4d photoelectrons, as compared with the Si 3s and 3p photoemission cross sections. Figure 4(*b*) shows spectra acquired with a photon energy of 80 eV, after the same Ar cleaning times as figure 4(*a*). At 80 eV, the photon energy is tuned to the Cooper minimum in the Nb 4d state. It can be seen that there is much less variation in the spectra. The reason is that only those states which are Nb 4d in nature undergo a Cooper minimum in cross section and hence, by comparing figures 4(*a*) and (*b*), we can conclude that these states are dominant very close to the Fermi edge. Figure 4(*c*) shows the effect of Ar cleaning on the insulating sample. The peak dominated by Si 3p (8 eV binding energy) is decreased in intensity after cleaning.

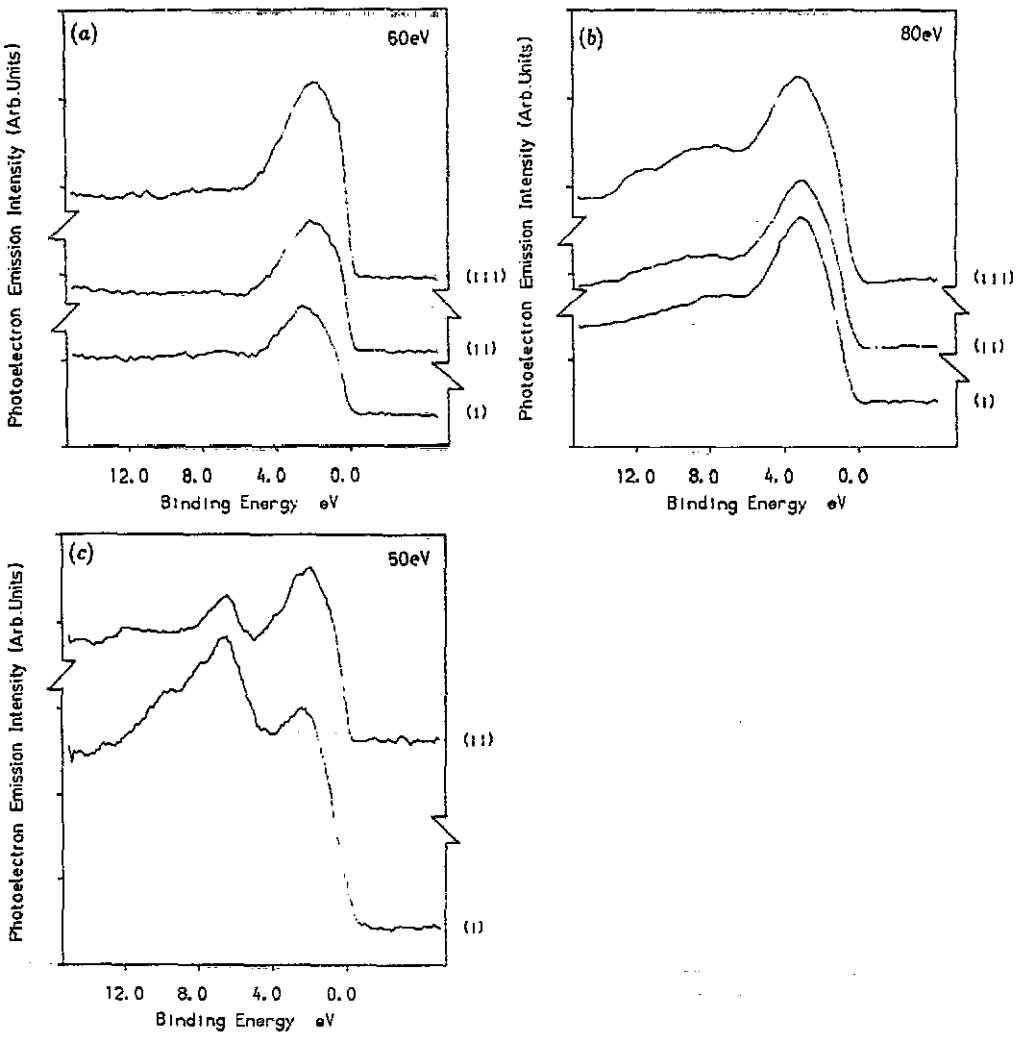

Figure 4. (*a*) EDC scans of the conducting a-NbSi sample (18.0 at.% Nb) after various stages of Ar cleaning. Photon energy = 60 eV using the high-energy monochromator; (i) as-sputtered; (ii) after 30 min cleaning at 1 kV; (iii) after a further 30 min cleaning at 2 kV. Note the sharpening of the Fermi edge as the cleaning continues. The increased area of the valence band peak is due to the increased Nb content (Nb 4d electrons have a larger photoemission cross section than Si 3p electrons). (*b*) EDS scans of conducting a-NbSi sample (18.0 at.% Nb) using the high-energy monochromator at same stages of cleaning as figure 3(*a*). Photon energy = 80 eV. Little change can be seen in the three spectra in contrast to those shown in figure 3(*a*). (*c*) EDC scans of insulating a-NbSi (1.5 at.% Nb) using the lower-energy monochromator: photon energy = 50 eV; (i) as-sputtered; (ii) after 30 min Ar cleaning at 2 kV. Note the reduction in size of the Si 3p peak and the creation of a Fermi edge.

CIS spectra of metallic and insulating samples after varying degrees of Ar bombardment are shown in figure 5. For the metallic case, shown in figure 5(*a*), the difference between photon energy and electron analysis energy is 7 eV, (corresponding to a binding energy relative to the Fermi level of 3 eV) so that this diagram presents the intensity of feature B in figure 3(*a*) plotted as a function of photon

energy. Note that the intensity of the Nb resonance increases with Ar bombardment, which implies an increase in the Nb concentration in agreement with the Auger spectra and the earlier discussion. The sharp spike on top of the resonance is caused by third-order photons exciting the Si 2p (binding energy 100 eV) level. The height of this peak reduces as the Nb resonance strengthens consistent with a reduction of Si concentration.

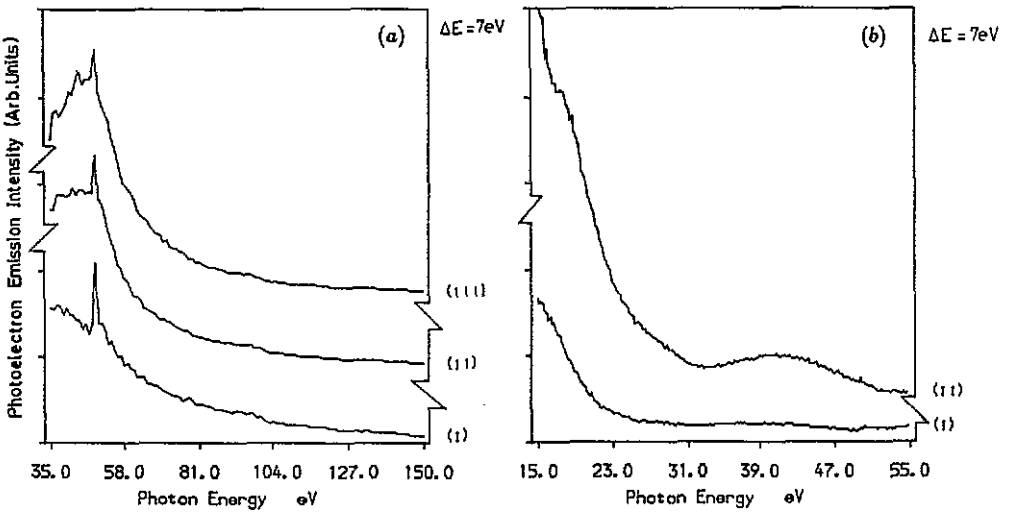

Figure 5. (*a*) CIS scans of the metallic (18.0 at.%) a-NbSi using the high-energy monochromator. Difference between photon energy and electron energy $\Delta E = 7$ eV. (i) As-sputtered; (ii) after 30 min Ar cleaning at 1 kV; (iii) after a further 30 min Ar cleaning at 2 kV. (*b*) CIS scans of insulating a-NbSi (1.5 at.% Nb) using the lower-energy monochromator. Difference between photon energy and electron energy $\Delta E = 7$ eV. (i) As-sputtered; (ii) after 30 min Ar cleaning at 2 kV. Note the increased size of the Nb resonance after cleaning.

CIS spectra acquired from the insulating sample are shown in figure 5(*b*). The difference between the electron analyser energy and photon energy was again set at 7 eV, so the same feature is investigated as in figure 4(*a*). The Nb resonance is much reduced as expected from the lower Nb concentration, but, as before, increases after Ar bombardment. In this case there is no sharp third-order peak as in figure 5(*a*) because these spectra were acquired on the lower-energy monochromator where third-order photons are of negligible intensity.

Weaver *et al* [21] found, by using calculated DOS and photoemission data, that in *crystalline* metal silicides the p–d hybridized bonding states account for the silicide stability and that these states tend to be a few eV below E_F. In the first transition series the states that are dominant in photoemission are the non-bonding 3d states (for Ca to Cu silicides) as there is little overlap with the Si derived states. For Ti through to Co there is an important d character within 3 eV of E_F. Hence, the electrical properties of these silicides are determined by the d states. The same authors also studied crystalline $NbSi_2$ with photoemission and found similarities with the silicides of the 3d transition metal series. These findings are in general agreement with the spectra presented in figure 3. As can be seen in figure 3(*a*), the Nb 4d resonance occurs over a wide range of energies, in accordance with the arguments advanced

by Weaver *et al*. However, a novel feature of the measurements presented here is the use of Cooper minima in such studies and a key point in the results is that data near the Cooper minimum ($h\nu \simeq 80$ eV) show a reduction in the sharpness of the Fermi edge. This suggests that virtually unhybridized Nb 4d states occur near the Fermi edge. These states will show fully fledged Cooper minima whereas mixed 4d–3p states which are also involved in the resonance will show less spectacular reductions at the energy of the Cooper minimum. Hence, the pure 4d states are more concentrated close to the Fermi edge in agreement with the conclusion of Weaver *et al* in their studies of crystalline $NbSi_2$.

4. Conclusions

By exploiting the variation of photoionization cross section with photon energy due to 4p→4d Nb resonant enhancement and the Nb 4d Cooper minimum, it has been possible to probe the partial DOS near the Fermi level in amorphous Nb_xSi_{1-x} prepared by *in situ* RF magnetron sputtering. Variation in surface composition with Ar ion exposure takes the system through an insulator–metal transition with consequent changes in the energy distribution curves. The metallic phase is characterized by virtually unhybridized Nb 4d states near the Fermi level in accord with previous studies on crystalline silicides. For the insulating phase, by way of contrast, there is no Fermi edge and little evidence for the Nb resonance.

Acknowledgments

The authors would like to thank R Bilsborrow, F M Quinn, T S Turner and other members of the Daresbury Laboratory staff for their help with the experimentation. We should also like to acknowledge the skilled support of A A M Croxon and M J Walker for making these experiments possible, and M F Mayeya and N Overend for their help in data collection. Finally, we thank the Science and Engineering Research Council and ICI for funding this project, and the referee for his probing comments on the initial text.

References

[1] Hertel G, Bishop D J, Spencer E G, Rowell J M and Dynes R C 1983 *Phys. Rev. Lett.* **50** 743
[2] Denhoff M and Gygax S 1986 *Phys. Rev.* B **34** 151
[3] Pounder N M and Howson M A 1991 *J. Phys.: Condens. Matter* **3** 2069
[4] Söldner K and Saemann-Ischenko G 1987 *Japan. J. Appl. Phys.* **26** 807
[5] Yeh J J and Lindau I 1985 *Atomic Data and Nuclear Data Tables* **32** 1
[6] Greig D, Gallagher B L, Howson M A, Law D S-L, Norman D and Quinn F M 1988 *Mater. Sci. Eng.* **99** 265
[7] Lowe A J, Greig D, Howson M A, Walker M J, Boghosian H H, Stevens R, Chen Y L, Law D S-L, Norman D, Quinn F M and Matthew J A D 1988 *J. Phys. C: Solid State Phys.* **21** L763
[8] Howells M R, Norman D, Williams G P and West J B 1978 *J. Phys. E: Sci. Instrum.* **11** 199
[9] Davis L E, MacDonald N C, Palmberg P W, Riach G E and Weber R E 1976 *Handbook of Auger Electron Spectroscopy* 2nd edn (Eden Prairie, MN: Physical Electronics Division, Perkin–Elmer Corp.)
[10] Briggs D and Seah M P 1983 *Practical Surface Analysis by Auger and X-ray Photoelectron Spectroscopy* (Chichester: Wiley)

[11] Zahorowski W, Šimůnek A, Wiech G, Söldner K, Knauf R, Saemann-Ischenko G 1987 *J. Physique Coll.* **48** C9 1205
[12] Wiech G, Zahorowski W, Šimůnek A, Šipr O 1989 *J. Phys.: Condens. Matter* **1** 5595
[13] Söldner K, Grassmann A, Saemann-Ischenko G, Zahorowski W, Šimůnek A and Wiech G 1989 *Z. Phys.* B **75** 59
[14] Morrell C, Baines J T M, Campbell J C, Diakun G P, Dobson B R, Greaves G N and Hasnain S S (ed) 1988 *Daresbury Laboratory EXAFS Users Manual*
Binstead N, Gurman S J and Campbell J W 1988 *Daresbury Laboratory EXCURV (88) Program*
[15] Hayes T M and Boyce J B 1982 *Solid State Phys.* **37** 173
[16] Kortright J B and Bienenstock A 1988 *Phys. Rev.* B **37** 2979
[17] Edwards A M, Fairbanks M C, Newport R J, Gurman S J and Davis E A 1989 *J. Non-Crystall. Solids* **113** 41
[18] Cardona M and Ley L (ed) 1978 *Photoemission in Solids I; General Principles* (New York: Springer) p 265
[19] Weaver J H, Moruzzi V L and Schmidt F A 1981 *Phys. Rev.* B **23** 2916
[20] Horache E, Fischer J E and Ruckman M W 1990 *Phys. Rev.* B **42** 11079
[21] Weaver J H, Franciosi A and Moruzzi V L 1984 *Phys. Rev.* B **29** 3293
[22] Joannopoulos J D and Cohen M L 1976 *Solid State Physics* vol 31, ed H Ehrenreich, F Seitz and D Turnbull (New York: Academic) p 71